Generation of optical skyrmions with tunable topological textures

Yijie Shen[a,*], Eduardo Casas Martínez[b], and Carmelo Rosales-Guzmán[c,d,*1]

[1a]*Optoelectronics Research Centre & Centre for Photonic Metamaterials, University of Southampton, Southampton SO17 1BJ, United Kingdom*

[b]*Instituto Nacional de Astrofísica, Óptica y Electrónica, Departamento de Óptica, Puebla, México*

[c]*Centro de Investigaciones en Óptica, A. C., Loma del Bosque 115, Col. Lomas del Campestre, 37150, León, Gto., México*

[d]*Wang Da-Heng Collaborative Innovation Center for Quantum Manipulation and Control, Harbin University of Science and Technology, Harbin 150080, China*

[*]*Correspondence: y.shen@soton.ac.uk (Y.S.); carmelorosalesg@cio.mx (C.R.G.)*

Abstract: In recent time, the optical-analogous skyrmions, topological quasiparticles with sophisticated vectorial structures in light, have received an increasing amount of interest. Here we propose theortically and experimentally a generalized family of these, the tunable optical skyrmion, unveiling a new mechanism to transform between various skyrmionic topologies, including Néel-, Bloch-, and anti-skyrmion types, via simple parametric tuning. In addition, a geometric Skyrme-Poincaré representation is proposed to visualize the complete topological evolution of tunable skyrmions, which we termed skyrmion torus. To generate experimentally the tunable optical skyrmions we implemented a digital hologram system based on a spatial light modulator, the results of which show great agreement with our theoretical prediction.

Key words: Skyrmion, topology, structured light, vector beams, spatial light modulator, orbital angular momentum.

INTRODUCTION

Skyrmions are topologically protected quasiparticles in high-energy physics and condensed matter with salient vectorial textures[1,2]. This concept was recently identified by the optics and photonics community as a cutting-edge topic. Recently, skyrmions were constructed in optical field as state-of-the-art optical structures and termed optical skyrmions[3]. These were first generated in the electric field of evanescent wave[3] followed by diverse forms constructed from different kinds of optical fields, such as, spin field of confined free-space waves[4,5], Stokes vectors of paraxial vector beams[6,7], magnetic vectors in propagating light pulses[8], and pseudospins in photonic crystals[9]. The creation of optical skyrmions has promising advanced applications in fields such as nanoscale metrology[10], deep-subwavelength microscopy[4], ultrafast vector imaging[11], and topological Hall devices[9], broadening the frontier of modern fundamental and applied physics.

The advancement skyrmions provide is mainly on their versatile topological textures, providing new degrees of freedom to shape vectorial fields and encode information. The skyrmionic configuration can be mapped into real-space magnetic materials and classified into diverse topologies[12,13], including Néel-type[14], Bloch-type[15], and anti-skyrmion[16]. However, the control of diverse topologies of optical skyrmions is an emerging topic still its infancy. As the first scheme of optical skyrmions, the evanescent electric fields on a plasmonic surface can only form Néel-type skyrmions[3,11]. One year ago, a study of plasmonic skyrmion controlled between Néel- and Bloch-types was reported[17], but, soon after, such Bloch-type skyrmion was disproved[18,19]. The loophole-free observation of Bloch-type optical skyrmion was reported very recently in optical chiral multilayers[20]. For the optical skyrmions in free space, Bloch-type skyrmion was proved in spin field of a tightly focused vortex beam[4]. And soon after, both Néel- and Bloch-type skyrmions were theoretically presented in Stokes vectors of paraxial vector beams[6] and electric-spin fields in tightly focused vector beams[5]. It is also of great importance to explore intermediate skyrmion-like states with extended topology, for instance, intermediate states between meron (half-charge skyrmion) and skyrmion in magnet[21,22] and light[10,23]. However, no experimental results have been reported for skyrmions with tunable topological textures in free space. Also, the concept of optical anti-skyrmion has never been realized yet.

In this paper, a closed-form expression is proposed to characterize a general class of optical skyrmions, where skyrmions with different textures (Néel-, Bloch-, and anti-skyrmion types) can be topologically transformed among each others via simple parametric tuning. Moreover, a novel geometrical model, skyrmion torus, is proposed to universally map the topological transformation of tunable optical skyrmions. Importantly, we experimentally generate the tunable optical skyrmions with all the topological types in structured vector beams controlled by a digital hologram system, showing great agreement with theoretical prediction.

THEORY

Topologies of skyrmions

Topological properties of a skyrmionic configuration can be characterized by the skyrmion number defined by[13]:

$$s = \frac{1}{4\pi}\iint_{\sigma} \mathbf{n}\cdot\left(\frac{\partial \mathbf{n}}{\partial x}\times\frac{\partial \mathbf{n}}{\partial y}\right)\mathrm{d}x\mathrm{d}y \tag{1}$$

where $\mathbf{n}(x,y)$ represents the vector field to construct a skyrmion and σ the region to confine the skyrmion, which can be infinity (for an isolated skyrmion) also can be a cell of a periodic distribution (for skyrmion lattices). The skyrmion number is an integer counting how many times the vector $\mathbf{n}(x,y) = \mathbf{n}(r\cos\theta, r\sin\theta)$ wraps around the unit sphere, as the mapping shown in Fig. 1(a). For mapping to the unit sphere, the vector can be given by $\mathbf{n} = (\cos\alpha(\theta)\sin\beta(r), \sin\alpha(\theta)\sin\beta(r), \cos\beta(r))$. Also, the skyrmion number can be separated into two integers:

$$\begin{aligned} s =& \frac{1}{4\pi}\int_0^{r_\sigma}\mathrm{d}r\int_0^{2\pi}\mathrm{d}\theta\frac{\mathrm{d}\beta(r)}{\mathrm{d}r}\frac{\mathrm{d}\alpha(\theta)}{\mathrm{d}\theta}\sin\beta(r) \\ =& \frac{1}{4\pi}[\cos\beta(r)]_{r=0}^{r=r_\sigma}[\alpha(\theta)]_{\theta=0}^{\theta=2\pi} = q\cdot m \end{aligned} \tag{2}$$

the polarity, $q = \frac{1}{2}[\cos\beta(r)]_{r=0}^{r=r_\sigma}$, indicates the direction of the vector down (up) at center $r = 0$ and up (down) at boundary $r \to r_\sigma$ for $q = 1$ ($q = -1$), and the vorticity, $m = \frac{1}{2\pi}[\alpha(\theta)]_{\theta=0}^{\theta=2\pi}$, controls the distribution of the transverse field components[24]. In the case of a helical distribution, an initial phase γ should be added, $\alpha(\theta) = m\theta + \gamma$. If we consider the transverse vector components at a given radius (or a given latitude angle β in the unit-sphere representation), the γ reveals the inclined angle of initial vector in the circular array, see Fig. 1(b). For the $m = 1$ skyrmion, the cases of $\gamma = 0$ and $\gamma = \pi$ are classified as Néel-type, and the cases of $\gamma = \pm\pi/2$ are Bloch-type. The case of $m = -1$ is anti-skyrmion.

Tunable optical skyrmions

In order to derive a closed-form expression that allows to tune between optical skyrmions with diverse topological textures via simple parameters, we start by a classic model of optical skyrmion, which was also also the first model of optical skyrmion. Namely, the skyrmionic vector field, $\mathbf{n} = (n_x, n_y, n_z)$, is constructed by the electric field vectors, $(E_x, E_y, E_z)^{\mathrm{T}}/|\mathbf{E}|$, in a confined surface plasmon polaritons (SPP) wave[3]:

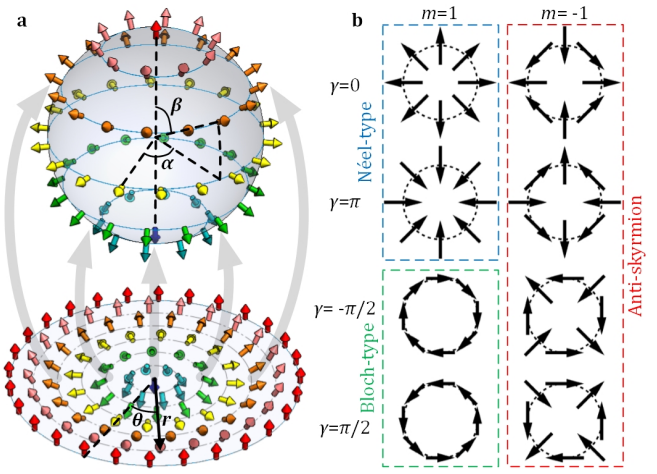

FIG. 1. (a) The mapping from a normal skyrmion configuration, constructed by the colored arrows, to the unit sphere representation. (b) Some basic cases of the transversely projected vector (E_x and E_y components) distribution at a given radius of the skyrmions with various values of m and γ.

$$\mathbf{n} = E_0 \mathrm{e}^{-|k_z|z}\sum_{n=1}^{N}\begin{pmatrix} -\frac{|k_z|\cos\theta_n}{k_\parallel}\sin\left(k_\parallel\mathbf{r}_\parallel\cdot\boldsymbol{\theta}_n\right) \\ -\frac{|k_z|\sin\theta_n}{k_\parallel}\sin\left(k_\parallel\mathbf{r}_\parallel\cdot\boldsymbol{\theta}_n\right) \\ \cos\left(k_\parallel\mathbf{r}_\parallel\cdot\boldsymbol{\theta}_n\right)\end{pmatrix} \tag{3}$$

where E_0 is a normalized amplitude, $k_\parallel$ and k_z are transverse (in-plane) and axial wavenumbers, $\mathbf{r}_\parallel = (x,y)$ and $\boldsymbol{\theta}_n = (\cos\theta_n, \sin\theta_n)$. The physical meaning of Eq. (3) is the superposition of N standing-wave SPPs along directions with equally distributed in-plane angles θ_n ($n = 1, 2, \cdots, N$). For common circular-shape skyrmions, N should be large enough, ideally $N \to \infty$. For the case of skyrmion lattice, N should be a integer related to the boundary geometry, e.g. $N = 3$ is set for simulating hexagonal skyrmion-lattice field with $\theta_n = [-\pi/3, 0, \pi/3]$[3]. Figure 2(a) shows a simulated result of skyrmionic vector distribution using Eq. (3). However, Eq. (3) can only represent Néel-type skyrmion (lattice). Here we propose a mathematically generalized form that breaks this limit:

$$\mathbf{n} = E_0 \mathrm{e}^{-|k_z|z}\sum_{n=1}^{N}\begin{pmatrix} -\frac{|k_z|\cos(\theta_n+\phi_1)}{k_\parallel}\sin\left(k_\parallel\mathbf{r}_\parallel\cdot\boldsymbol{\theta}_n\right) \\ -\frac{|k_z|\sin(\theta_n+\phi_2)}{k_\parallel}\sin\left(k_\parallel\mathbf{r}_\parallel\cdot\boldsymbol{\theta}_n\right) \\ \cos\left(k_\parallel\mathbf{r}_\parallel\cdot\boldsymbol{\theta}_n\right)\end{pmatrix} \tag{4}$$

Compared with Eq. (3), Eq. (4) has two additional parameters, ϕ_1 and ϕ_2, the control of which can drive the skyrmionic vector field to cover all the three classic types of topologies: Néel-type for $\phi_1 = \phi_2 = 0$ or $\phi_1 = \phi_2 = \pi$, Bloch-type for $\phi_1 = \phi_2 = \pi/2$ or

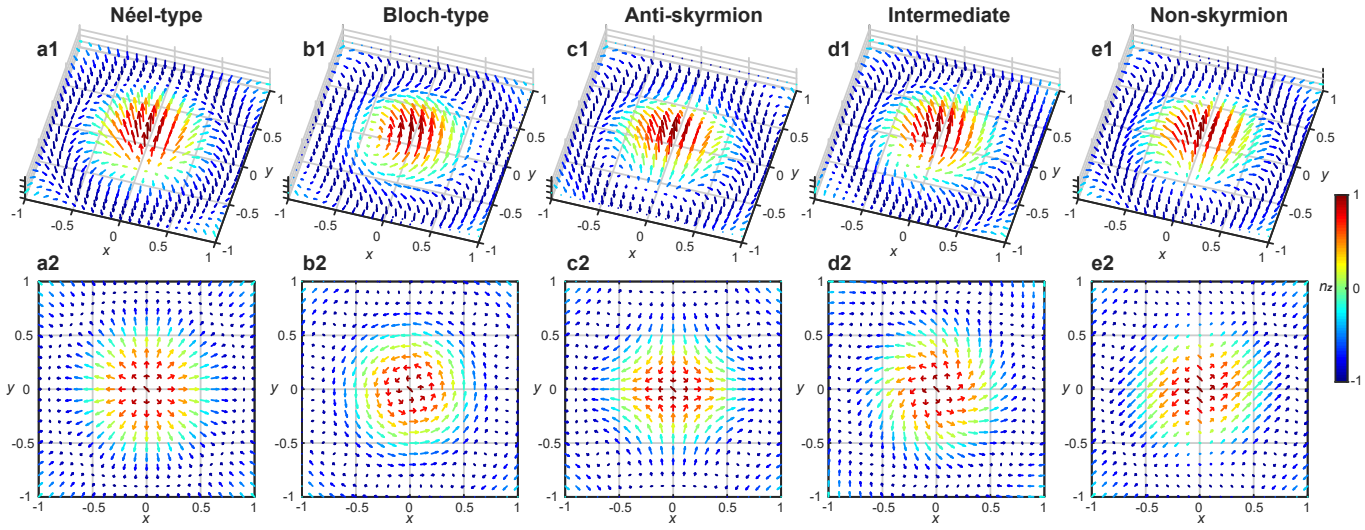

FIG. 2. (a-d) The simulated results of (a1-d1) the 3D vector distributions, (n_x, n_y, n_z), and (a2-d2) the transverse component vectors, (n_x, n_y), for tunable optical skyrmions with diverse topological textures of Néel-type (a, $\phi_1 = \phi_2 = 0$), Bloch-type (b, $\phi_1 = \phi_2 = \pi/2$), anti-skyrmion (c, $\phi_1 = 0$, $\phi_2 = \pi$), an intermediate state (d, $\phi_1 = \phi_2 = \pi/4$), and a non-skyrmion (e, $\phi_1 = 0$ $\phi_2 = \pi/2$), respectively.

$\phi_1 = \phi_2 = 3/\pi/2$, and anti-skyrmion for $|\phi_1 - \phi_2| = \pi$. Numerically simulated results of Eq. (4) for these three topological types are shown in Figs. 2a-2c. In general, ϕ_1 and ϕ_2 act as the parameters to dynamically tune the topological textures among the three typical ones.

It is worth noting that the Néel-type can continuously deform into Bloch-type textures. In general, the intermediate skyrmions can be interpreted by Eq. (4) when $\phi_1 = \phi_2 = \phi \in [0, 2\pi]$ ($\phi = 0, \pi$ for Néel-type and $\phi = \pi/2, 3\pi/2$ for Bloch type), see **Video 1** for a movie shown this evolution and an example of intermediate skyrmion in Fig. 2d. However, the anti-skyrmion is impossible to deform into Néel or Bloch skyrmion, because they have different topological protection (opposite vorticity). When the evolution goes from Néel-type or Bloch-type to an anti-skyrmion, the vector field must meet a boundary state of non-skyrmion, an example of which is shown in Fig. 2e. In the non-skyrmion, its transverse component vectors only have a single 45° orientation, thus it is not a skyrmion (the skyrmion require the transverse component covering full azimuth). See **Video 2** (**Video 3**) for the evolution from a Bloch (Néel) skyrmion to an anti-skyrmion.

The mathematical representation of Eq. (4) is correct for tunable optical skyrmion, but its experimental realization is still cumbersome. Attempting to use SPP to generate tunable skyrmions, as described by Eq. (4), the two parameters ϕ_1 and ϕ_2 would induce extreme conditions that are hard to fulfill, as a stable SPP field requires rigorous conditions than a free-space light field.

Importantly, recent advancements had made possible the successful realisation of optical skyrmions of different optical vector fields in both matter and free space but are still limited to few topological textures[4–6,9]. These advancements allows to propose a practical scheme for the generation of tunable optical skyrmions in free space, via the Stokes vectors of structured vector beams. The Stokes vector $\mathbf{s} = (s_1, s_2, s_3)$ can represent an arbitrary state of polarization, as points on the surface of unit-radius sphere known as the Poincaré sphere[25]. In spherical coordinates, the optical field $\mathbf{\Psi} = \cos(\theta/2)e^{-i\varphi/2}\mathbf{R} + \sin(\theta/2)e^{i\varphi/2}\mathbf{L}$, where $\mathbf{R}$ and $\mathbf{L}$ represent right- and left-handed circularly polarized (RCP and LCP) eigenstates, respectively, is represented as $\mathbf{s} = (\cos\varphi\sin\theta, \sin\varphi\sin\theta, \cos\theta)$. In order to construct skyrmions by Stokes vector, we need to first construct a vector beam with customized spatial modes of the form,

$$\mathbf{\Psi}(x,y) = \psi_1(x,y)\mathbf{R} + \psi_2(x,y)\mathbf{L}. \tag{5}$$

The spatial modes ψ_1 and ψ_2 should have the same form of the tunable skyrmion, given by Eq. (4), that is,

$$\psi_1(x,y) = \cos[\theta(x,y)/2]e^{-i\varphi(x,y)/2} \tag{6}$$

$$\psi_2(x,y) = \sin[\theta(x,y)/2]e^{i\varphi(x,y)/2}, \tag{7}$$

with

$$\theta(x,y) = \cos^{-1}[n_z(x,y)] \tag{8}$$

$$\varphi(x,y) = \sin^{-1}\left[\frac{n_y(x,y)}{\sin\theta(x,y)}\right] = \cos^{-1}\left[\frac{n_x(x,y)}{\sin\theta(x,y)}\right] \tag{9}$$

where, (n_x, n_y, n_z) is exactly based on theoretical tunable skyrmion of Eq. (4). We can now tailor vector beams to realize tunable skyrmions via their Stokes

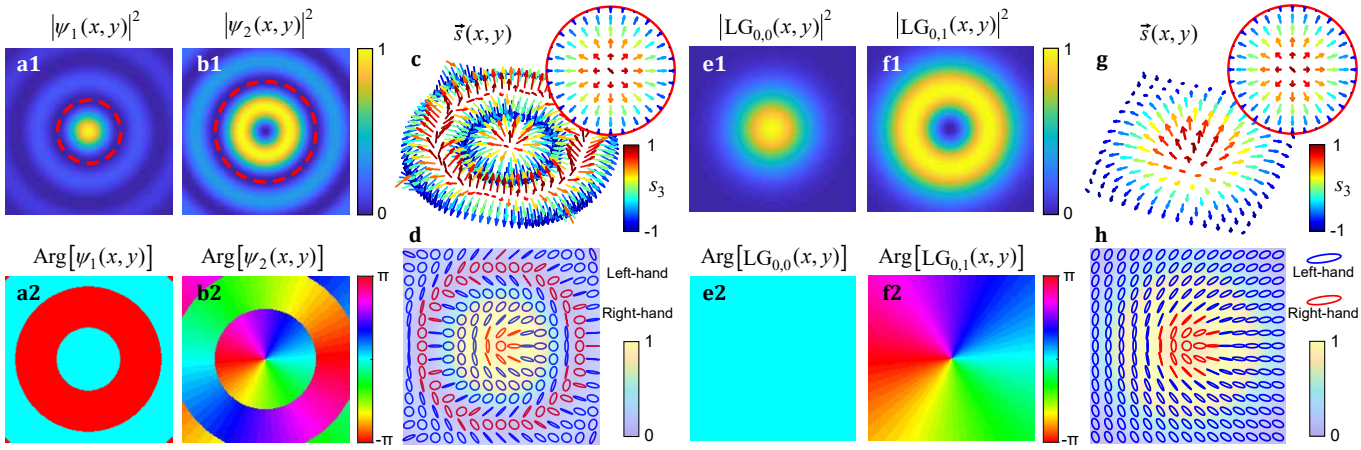

FIG. 3. (a,b) Intensity (a1,b1) and phase (a2,b2) distributions of $\psi_1(x,y)$ (a) and $\psi_1(x,y)$ (b) for the case of $\phi_1 = \phi_2 = 0$, the red-dash lines mark the effective regions to induce the main topological texture of optical skyrmion. (c,d) The skyrmion in Stokes vector field with transverse component inset (c) and the intensity and polarization distributions (d) of the corresponding vector beam. (e,f) Intensity (e1,e2) and phase (f1,f2) distributions of $LG_{0,0}(x,y)$ (e) and $LG_{0,1}(x,y)$ (f) modes at beam waist plane. (g) The skyrmion in Stokes vector field with transverse component inset (g) and the intensity and polarization distributions (h) of the LG based vector beam.

vector fields. As a way of example, a numerical simulation of the Néel-type skyrmionic vector beam, for which $\phi_1 = \phi_2 = 0$, is shown in Fig. 3. The spatial modes $\psi_1(x,y)$ and $\psi_2(x,y)$ are shown in Figs. 3(a,b), which share the same amplitude and phase distributions as that of the transverse zero-order and first-order Bessel modes, respectively. Note that although they share the same form, $\psi_1(x,y)$ and $\psi_2(x,y)$ are derived based on surface plasma fields located on a 2D surface, whereas Bessel beams are propagating beams. The distributions of Stokes vectors, intensity and polarizations are shown in Figs. 3(c,d), respectively, where the central region of a Néel-type skyrmion texture and full states of polarization can be observed. The simulation results also show that the effective regions that contributes to the main hedgehog-like vector texture are the central lobes of the zero- and first-order Bessel modes, as marked by red-dashed lines in Figs. 3(a,b). While the side lobes, far away the skyrmion center, of the Bessel beams contribute to the repeating radial reversal vector structure that does not impact on the skyrmion topology. Therefore, we can replace the zero- and first-order Bessel modes by the fundamental Gaussian and first-order Laguerre-Gaussian (LG) modes, i.e. $LG_{0,0}$ and $LG_{0,1}$ shown in Fig. 3(e,f). The Stokes vector field of the corresponding LG-based vector beam given by Eq. (5) shows a perfect Néel-type skyrmion, as evinced in Figs. 3(c,d). Note that, in contrast to the nondiffracting Bessel modes, the LG modes are diffracting beams, here we observe the skyrmions at the beam waist plane of the beams.

Skyrmion torus and Skyrme-Poincaré model

In this section we present an elegant graphical model, skyrmion torus, to depict the general topological state transformation of tunable skyrmion onto a torus. Without loss of generality, setting $\phi_1 = \Phi \in [0, 2\pi]$ and $(\phi_2 - \phi_1) = \Theta \in [-\pi, \pi]$, we can regard Φ and Ψ as angles of toroidal and poloidal directions, respectively, to map the general topological states of skyrmions to corresponding points on a torus, as shown in Fig. 4. For $\Theta = 0$, the skyrmion transforms between Néel ($\Phi = 0, \pi$) and Bloch ($\Phi = \pm\pi/2$), which are represented on

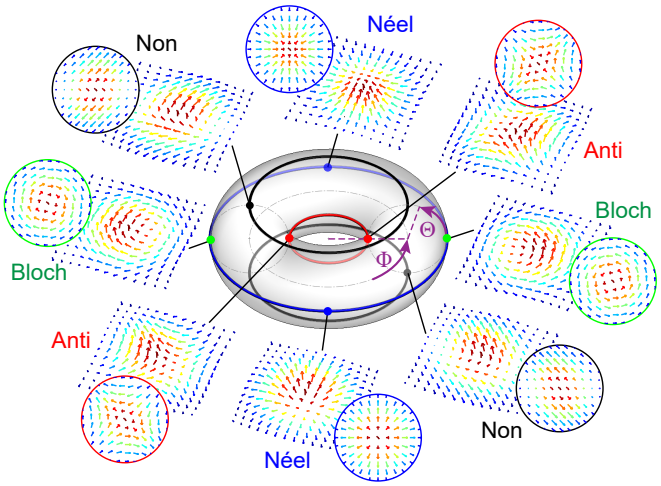

FIG. 4. The skyrmion torus to represent universal topological evolution of tunable optical skyrmion, with special topology as a point on it: Red points, Néel-type; green points, Bloch-type; Blue points (the poles), anti-skyrmion.

the big toroidal circle. The anti-skyrmions with diverse orientations ($\Theta = \pm\pi$) are located at the small toroidal circle. The two middel toroidal circles at top and bottom represent various non-skyrmion states. Any route of toroidal circle represents a skyrmion-number-invariant transformation. Any route of poloidal circle on the torus describes a dynamic tuning between a Néel or Bloch skyrmion ($s = 1$) and an anti-skyrmion ($s = -1$).

The skyrmion torus to represent skyrmionic texture evolution has an intriguing relation to the OAM Poincaré sphere to represent OAM evolution of a vortex beam. Based on the methods introduced in last section, we can derive the parametric form of corresponding vector beam dependent on Φ and Θ:

$$\mathbf{\Psi} = \Psi_0 \mathbf{R} + \left[\cos(\Theta/2)e^{-i\Phi/2}\Psi_{-1} + \sin(\Theta/2)e^{i\Phi/2}\Psi_1\right]\mathbf{L} \tag{10}$$

where Ψ_0 is zero-order Bessel (or fundamental Gaussian) mode and $\Psi_{\pm 1}$ are $\pm$1th-order Bessel modes (or LG modes) carrying opposite OAM with ± 1 topological charges. And the spatial mode of LCP component is exactly the form of conventional OAM Poincaré sphere[26], driven by the longitude and latitude angles Φ and Θ, revealing the OAM conversion between ± 1 topological charges. In OAM Poincaré sphere, when $\Theta = 0$, the scalar mode always represents an OAM with single topological charge, independent with the angle of Φ. That is why the OAM evolution is mapped on a sphere and the pure OAM state is represented on the pole. However, the skyrmionic vector beam add new degree of freedom to distinguish the Φ-dependent states with different Néel and Bloch textures when $\Theta = 0$. Therefore the combined skyrmionic vector texture should be mapped onto a torus. Therefore the torus mapping acts as an useful tool to tailor general skyrmionic topological transformations, akin to the Poincaré sphere for tailoring OAM. As such, many related applications, such as spin-orbit conversion, geometric phase transition, encoding and communication[25,27,28], are expected to be analogously studied in optical skyrmion.

EXPERIMENT

In order to realize experimentally the tunable optical skyrmions, we implemented a highly stable optical setup capable to generate arbitrary optical beams with almost any state of polarisation and spatial profile[29], which is schematically shown in Fig. 5 . Such optical setup comprises the use of a Spatial Light Modulator (SLM) for arbitrary control of the spatial distribution of the optical field[30]. The setup starts with a horizontally polarised HeNe (632.8 nm) laser beam, collimated and expanded to fully cover the liquid crystal screen of

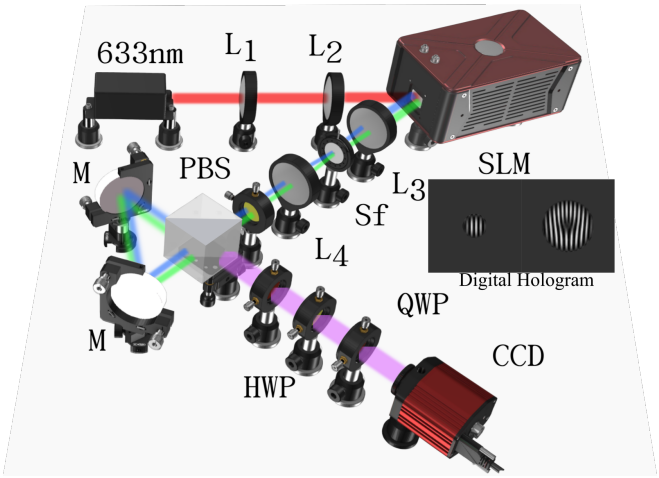

FIG. 5. Schematic representation of the optical setup implemented to generate tunable optical skyrmions. L_1 – L_4:lenses, PBS: Polarizing Beam Splitter, SLM:Spatial Light Modulator HWP: Half-Wave plate, QWP: Quarter-Wave Plate, M: Mirror, SF: Spatial Filter, CCD: Charge Coupled Device Camera

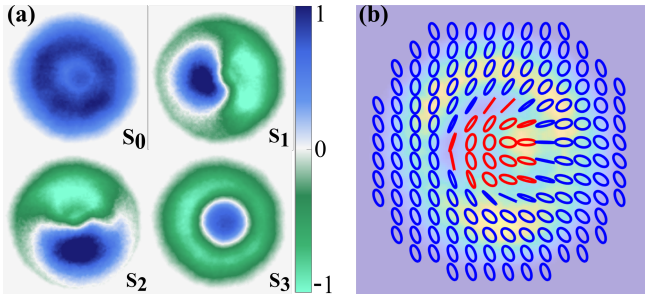

FIG. 6. Experimentally reconstructed (a) Stokes parameters and (b) intensity distribution of the vector field overlapped with its corresponding polarisation distribution.

the SLM. The screen of the SLM is digitally split into two independent screens, each of which is addressed with an independent digital hologram that generates, in the first diffraction order, two independent optical fields. The holograms are chosen according to the desired skyrmion as given by Eq. 10. To better approximate the Bessel or LG modes, we modulated both, the amplitude and phase of the desired modes using complex amplitude modulation (see[30] for additional details). For example, to generate skyrmions, ($\Theta = 0$), only the second term of the left-handed polarisation component is present, *i.e.*, Ψ_1. Hence, on one side of the SLM we encode the mode Ψ_0 (fundamental Gaussian mode) and on the other side the mode Ψ_1 (First order Bessel or LG mode). An example of the encoded hologram is shown as an inset in Fig. 5. It can also be seen here that each hologram is superimposed with a linear grating to separate the different diffraction orders and filter the first diffraction using a telescope formed by two lenses and a spatial filter located in the focal

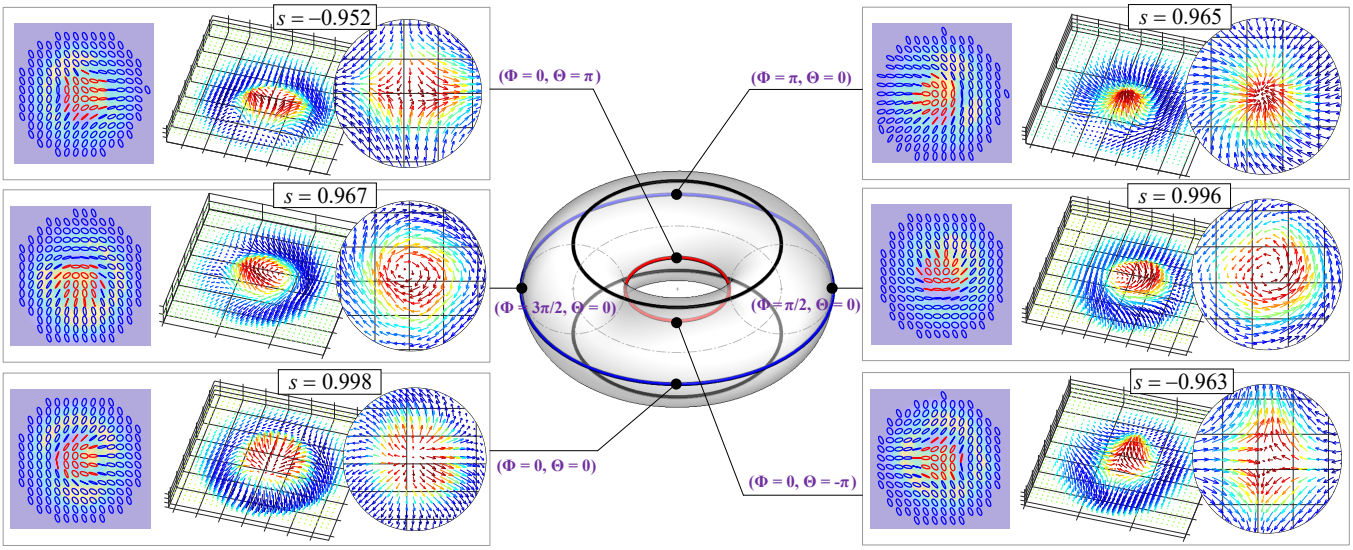

FIG. 7. Experimental results of tunable Stokes skyrmions with controlled topological textures corresponding to selective points on skyrmion torus (see gray boxes), each box include the measured intensity and polarization distribution of the skyrmionic beam, the vector distribution of the Stokes skyrmions, and the zoom-in planform of the vector field for clearly distinguishing the topological texture. Numerically calculated skyrmion numbers are noted in divers panels correspondingly.

plane of the first lens. The two optical fields are then redirected to a common-path triangular Sagnac interferometer comprising a Polarising Beam Splitter (PBS) and two mirrors. Prior to entering the interferometer, both beams are rotated to a diagonal polarisation state. In this way, when both beams enter the interferometer, after traversing the PBS, each of them is separated into two new beams with orthogonal linear polarisation states, horizontal and vertical, traveling along opposite optical paths. After a round trip, all four beams exit the interferometer from the opposite side of the PBS, two with horizontal polarization and two with vertical. Finally, the horizontal polarisation component of one of the beams is aligned co-axially with the vertical polarisation component of the other beam. To improve the coaxial superposition, a fine tuning is performed digitally via the period of the linear gratings encoded on each digital hologram. Importantly, optical aberrations produced by the screen of the SLM, which are not perfectly flat, induce small deviations between the experimental and theoretical results. Nonetheless, such aberrations can be removed by adding a correction mask to the SLM. Such correction lies beyond the scope of this manuscript since our purpose is just to demonstrate the concept.

The experimental reconstruction of the optical skyrmions was achieve through Stokes polarimetry, more specifically, through the reconstruction of the Stokes parameters S_0, S_1, S_2 and S_3, which were computed from a set of intensity measurements. To this end, a second stage was build at the output port of the interferometer, where a series of phase retarders and a Charge-Coupled Device (CCD) camera allowed to measure the required intensities, from which the Stokes parameters where reconstructed using the relations,

$$\begin{aligned} S_0 &= I_H + I_V, & S_1 &= 2I_H - S_0, \\ S_2 &= 2I_D - S_0, & S_3 &= 2I_R - S_0, \end{aligned} \tag{11}$$

where, I_H, I_V, I_D and I_R represent the intensity of the horizontal, vertical, diagonal and right-handed polarisation components, respectively. To experimentally measure I_H, I_V and I_D we passed the optical field through a linear polariser set at 0°, 45° and 95°, respectively, while the intensity of the I_R polarisation component was acquired by passing it simultaneously through a QWP at 45° and a linear polariser at 90° (see[31] for further details). Figure 6(a) show an example of the experimental Stokes parameters along with the intensity profile overlapped with its corresponding polarization distribution, Fig. 6(b), for the specific case $\phi_1 = \phi_2 = 0$. In this example, the beam center includes a pure RCP state ($S_3 = 1$), represented by a dark blue color. This is because the beam is composed by a coaxial superposition of the LCP fundamental Gaussian mode and LCP LG mode, which has a null at its centre. Thus the point in the centre of the composed mode exists as a pure RCP (S3=+1) state, which exactly corresponds to a generic C-point[32]. The holograms used in this example are displayed as insets in Fig. 5 (Digital Hologram) and correspond, from left to right, to the fundamental Gaussian mode and the first order LG mode. Importantly, all topological structures represented on the torus can be chosen according to Eq.(10), by simply changing the holograms displayed on the SLM.

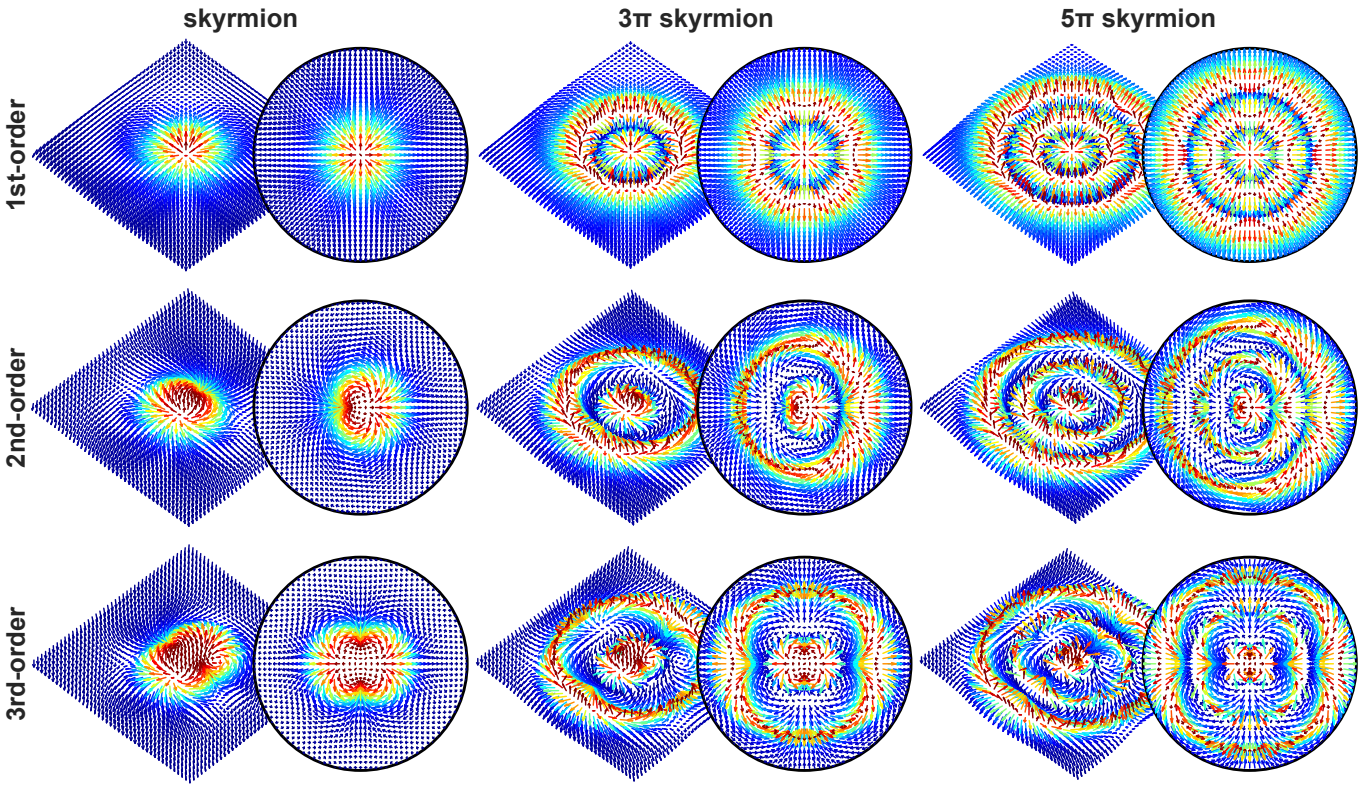

FIG. 8. Theoretical results of complex higher-order $k\pi$ skyrmions in Stokes vector field of the mode $\mathbf{\Psi}_{p,\ell}$, the inset of each panel shows corresponding transverse component distribution. The first, second, and third rows correspond to the results of vorticity numbers of 1, 2, and 3, for the parameter used as $\ell = 1$, 2, and 3, respectively. The first, second, and third columns correspond to the results of radial twist of 1π, 3π, and 5π, for the parameter used as $p = 0$, $p = 1$, and $p = 2$, respectively.

With our digital hologram system, we realized a controlled generation of Stokes skyrmions with arbitrary topological textures on the skyrmion torus. Figure 7 shows our experimentally generated LG-based results of tunable Stokes skyrmions on typical points of skyrmion torus, including the measured intensity and polarization distributions, Stokes vector fields, and a zoom-in of the central region of the vector field for clearly distinguishing the topological textures. From our experimental results, we can clearly identify the textures (hedgehog for Néel skyrmion, vortex for Bloch skyrmion, and saddle for anti-skyrmion). Importantly, the vector field shows small experimental deviation from the theoretical predictions, however, these errors can be tolerated since we are interested in the 3D topology of the skyrmionic structure, where no significant deviations are observed. For a verification, we can numerically calculate the skyrmion numbers of our experimental results using Eq.(1), the results are noted in Fig. 7. The experimental skyrmion numbers agree well with the corresponding theoretical predictions: anti-skyrmions for $s = -1$; Bloch and Neel skyrmions for $s = 1$. Additional experimental results are shown as supplementary materials in **Video 4** and **Video 5** for both cases based on LG and Bessel-Gaussian modes.

DISCUSSION

Although the generalized tunable optical skyrmion model is inspired from the case of SPP electric field, and realized by Stokes vector field, it is not limited in these cases and can be freely extendable. Because the new concept of tunable skyrmion has a universal mathematical parametrization for generalized topology, the vector can refer to other kinds of optical field of structured light for the further exploration. For example, we can also use spin vectors in a tightly focused beam[4,5], electric or magnetic vectors in a propagating structured pulse[8], and pseudospins in nonlinear media[9]. It is also a exciting direction to create more quasiparticle with complex topological states beyond skyrmions, such as skyrmion bags[33] and skyrmion tubes[34], meron and bimeron[35–37], into structured light. Even though in this work, we used an SLM to generate skyrmionic beams, Digital Mirror Devices represent an alternative means to generated them, which present several advantages over SLMs, such as, their high refresh rates, polarisation independence and low cost[31].

The above results only show the cases with skyrmion number of ± 1. Nonetheless, our model can be easily extended to higher-order skyrmions with increas-

ingly complex topology, that are hard to realize with previous optical skyrmions methods. To this end, we only need to replace the single-topological-charge vortex mode $\Psi_{\pm}$ in Eq. (10) into the general LG modes with both radial and azimuthal indices $\psi_{p,\ell}$, more precisely,

$$\mathbf{\Psi}_{p,\ell} = \psi_{0,0}\mathbf{R} + \left[\cos(\Theta/2)e^{-i\Phi/2}\psi_{p,-\ell} + \sin(\Theta/2)e^{i\Phi/2}\psi_{p,\ell}\right]\mathbf{L} \tag{12}$$

This equation represents more general topological skyrmions in its Stokes fields. The index p controls the radial multi-twist structure in skyrmion, i.e. the so-called skyrmionium or $k\pi$ target skyrmion[38], and the index ℓ controls higher vorticity numbers in skyrmion, i.e. the structure previously called higher-order skyrmions[9]. A set of results of Néel-type complex higher-order $k\pi$ skyrmions based on Eq. (12) are shown in Fig 8.

It is worth mentioning that even though the skyrmions studied in this work share some similarities with full Poincaré beams[39–42] and their associated polarisation singularities[32,43]there are clear differences. Thus it is worth unveiling the relationship between the new concept of tunable topological skyrmions and Poincaré beams. For instance, the a Néel-to-Bloch skyrmion corresponds to a Poincaré beams with a lemon-type C-point, whereas an anti-skyrmion corresponds to a start-type C-point. Therefore, it is still interesting to study the relationship between other kinds of complex skyrmions and Poincaré beams with polarization singularities.

Finally, even though proposing novel techniques for the generation of diverse topological skyrmions is of greta relevance, another interesting direction to is the study of novel techniques for the characterisation of such structures. More precisely, for a given skyrmionic beam, it is desired to precisely quantify its topological state on the skyrmion torus with coordinate (Φ, Θ). We can anticipate that some recent advanced measurement method for vector beams, such as state tomography method[44] represent a promising avenue to this.

CONCLUSION

Conclusively, we proposed an extended family of tunable optical skyrmion, enabling flexible transformation among various kinds of skyrmionic topological textures. A graphical model, skyrmion torus, is proposed to universally represent the topological evolution of tunable optical skyrmion. We experimentally generated such tunable optical skyrmions in Stokes vector fields of customized vector beams from a well-designed digital hologram system. This is the first-know experimental generation of topology-tunable optical skyrmions in free space, also the first realization of optical anti-skyrmions. Our methods are easily extended to higher-order topology to provide a new platform for optical information storage, communication, and cryptography using skyrmionic topological states of light.

Finally, it has come to our attention that, when we were preparing our manuscript, an independent experiment that explored optical skyrmion in a vector beam was reported[45]. It focused on a 3D skyrmion structure, while we focused the tunability of 2D skyrmion structures. In contrast to conventional 2D skyrmion (spin textures confined in a 2D plane), the 3D skyrmion, as a generalized form, can include multiple topological textures in multiple transverse plane upon propagation. Therefore, it is also a meaningful direction to improve our approach to control topologically tunable 3D skyrmions in the future.

FUNDING SOURCES

This work is funded by National Natural Science Foundation of China (61975047).

SUPPORTING INFORMATION

The Supporting Information is available free of charge online at https://pubs.acs.org/:

Video 1: Topology-tunable skyrmion transformed between Néel- and Bloch-types.

Video 2: Topology-tunable skyrmion transformed between Bloch- and Anti-types.

Video 3: Topology-tunable skyrmion transformed between Néel- and Anti-types.

Video 4: Experimental results of topology-tunable skyrmion controlled on skyrmion torus based on LG mode.

Video 5: Experimental results of topology-tunable skyrmion controlled on skyrmion torus based on Bessel-Gaussian mode.

REFERENCES

[1] Börge Göbel, Ingrid Mertig, and Oleg A Tretiakov, "Beyond skyrmions: Review and perspectives of alternative magnetic quasiparticles," Phys. Rep. **895**, 1–28 (2021).

[2] Albert Fert, Nicolas Reyren, and Vincent Cros, "Magnetic skyrmions: advances in physics and potential applications," Nat. Rev. Mater. **2**, 1–15 (2017).

[3] S Tsesses, E Ostrovsky, K Cohen, B Gjonaj, NH Lindner, and G Bartal, "Optical skyrmion lattice in evanescent electromagnetic fields," Science **361**, 993–996 (2018).

[4] Luping Du, Aiping Yang, Anatoly V Zayats, and Xiaocong Yuan, "Deep-subwavelength features of photonic skyrmions in a confined electromagnetic field with orbital angular momentum," Nat. Phys. **15**, 650–654 (2019).

[5] Rodrigo Gutiérrez-Cuevas and Emilio Pisanty, "Optical polarization skyrmionic fields in free space," J. Opt. **23**, 024004 (2021).

[6] Sijia Gao, Fiona C Speirits, Francesco Castellucci, Sonja Franke-Arnold, Stephen M Barnett, and Jörg B Götte, "Paraxial skyrmionic beams," Phys. Rev. A **102**, 053513 (2020).

[7] Wenbo Lin, Yasutomo Ota, Yasuhiko Arakawa, and Satoshi Iwamoto, "Microcavity-based generation of full poincaré beams with arbitrary skyrmion numbers," Phys. Rev. Res. **3**, 023055 (2021).

[8] Yijie Shen, Yaonan Hou, Nikitas Papasimakis, and Nikolay I Zheludev, "Supertoroidal light pulses as electromagnetic skyrmions propagating in free space," Nat. Commun. **12**, 1–9 (2021).

[9] Aviv Karnieli, Shai Tsesses, Guy Bartal, and Ady Arie, "Emulating spin transport with nonlinear optics, from high-order skyrmions to the topological hall effect," Nat. Commun. **12**, 1–9 (2021).

[10] Yanan Dai, Zhikang Zhou, Atreyie Ghosh, Roger SK Mong, Atsushi Kubo, Chen-Bin Huang, and Hrvoje Petek, "Plasmonic topological quasiparticle on the nanometre and femtosecond scales," Nature **588**, 616–619 (2020).

[11] Timothy J Davis, David Janoschka, Pascal Dreher, Bettina Frank, Frank-J Meyer zu Heringdorf, and Harald Giessen, "Ultrafast vector imaging of plasmonic skyrmion dynamics with deep subwavelength resolution," Science **368** (2020).

[12] XZ Yu, Yoshinori Onose, Naoya Kanazawa, JH Park, JH Han, Yoshio Matsui, Naoto Nagaosa, and Yoshinori Tokura, "Real-space observation of a two-dimensional skyrmion crystal," Nature **465**, 901–904 (2010).

[13] Naoto Nagaosa and Yoshinori Tokura, "Topological properties and dynamics of magnetic skyrmions," Nat. Nanotechnol. **8**, 899–911 (2013).

[14] István Kézsmárki, Sándor Bordács, Peter Milde, E. Neuber, L.M. Eng, J.S. White, Henrik M. Rønnow, C.D. Dewhurst, M. Mochizuki, K. Yanai, H. Nakamura, D. Ehlers, V. Tsurkan, and A. Loidl, "Néel-type skyrmion lattice with confined orientation in the polar magnetic semiconductor gav 4 s 8," Nat. Mater. **14**, 1116–1122 (2015).

[15] Dustin A Gilbert, Brian B Maranville, Andrew L Balk, Brian J Kirby, Peter Fischer, Daniel T Pierce, John Unguris, Julie A Borchers, and Kai Liu, "Realization of ground-state artificial skyrmion lattices at room temperature," Nat. Commun. **6**, 1–7 (2015).

[16] Ajaya K Nayak, Vivek Kumar, Tianping Ma, Peter Werner, Eckhard Pippel, Roshnee Sahoo, Franoise Damay, Ulrich K Rößler, Claudia Felser, and Stuart SP Parkin, "Magnetic antiskyrmions above room temperature in tetragonal heusler materials," Nature **548**, 561–566 (2017).

[17] Chunyan Bai, Jian Chen, Yuxing Zhang, Dawei Zhang, and Qiwen Zhan, "Dynamic tailoring of an optical skyrmion lattice in surface plasmon polaritons," Opt. Express **28**, 10320–10328 (2020).

[18] Tim Meiler, Bettina Frank, and Harald Giessen, "Dynamic tailoring of an optical skyrmion lattice in surface plasmon polaritons: comment," Opt. Express **28**, 33614–33615 (2020).

[19] Chunyan Bai, Jian Chen, Dawei Zhang, and Qiwen Zhan, "Dynamic tailoring of an optical skyrmion lattice in surface plasmon polaritons: reply," Opt. Express **28**, 33616–33618 (2020).

[20] Qiang Zhang, Zhenwei Xie, Luping Du, Peng Shi, and Xiaocong Yuan, "Bloch-type photonic skyrmions in optical chiral multilayers," Phys. Rev. Res. **3**, 023109 (2021).

[21] XZ Yu, W Koshibae, Y Tokunaga, K Shibata, Y Taguchi, N Nagaosa, and Y Tokura, "Transformation between meron and skyrmion topological spin textures in a chiral magnet," Nature **564**, 95–98 (2018).

[22] Hariom Jani, Jheng-Cyuan Lin, Jiahao Chen, Jack Harrison, Francesco Maccherozzi, Jonathon Schad, Saurav Prakash, Chang-Beom Eom, Ariando Ariando, Thirumalai Venkatesan, and Paolo G. Radaelli, "Antiferromagnetic half-skyrmions and bimerons at room temperature," Nature **590**, 74–79 (2021).

[23] Lin Xiong, Yutao Li, Dorri Halbertal, Michael Sammon, Zhiyuan Sun, Song Liu, James H Edgar, Tony Low, Michael M Fogler, Cory R Dean, Andrew J. Millis, and D. N. Basov, "Polaritonic vortices with a half-integer charge," Nano Lett. **21**, 9256–9261 (2021).

[24] XS Wang, HY Yuan, and XR Wang, "A theory on skyrmion size," Communications Physics **1**, 1–7 (2018).

[25] Carmelo Rosales-Guzmán, Bienvenu Ndagano, and Andrew Forbes, "A review of complex vector light fields and their applications," J. Opt. **20**, 123001 (2018).

[26] Miles J Padgett and Johannes Courtial, "Poincaré-sphere equivalent for light beams containing orbital angular momentum," Opt. Lett. **24**, 430–432 (1999).

[27] Yijie Shen, Xuejiao Wang, Zhenwei Xie, Changjun Min, Xing Fu, Qiang Liu, Mali Gong, and Xiaocong Yuan, "Optical vortices 30 years on: Oam manipulation from topological charge to multiple singularities," Light Sci. Appl. **8**, 1–29 (2019).

[28] Mark R Dennis and Miguel A Alonso, "Swings and roundabouts: optical poincaré spheres for polarization and gaussian beams," Philos. Trans. R. Soc. A **375**, 20150441 (2017).

[29] Benjamin Perez-Garcia, Carlos López-Mariscal, Raul I. Hernandez-Aranda, and Julio C. Gutiérrez-Vega, "On-demand tailored vector beams," Appl. Opt. **56**, 6967–6972 (2017).

[30] Carmelo Rosales-Guzmán and Andrew Forbes, *How to shape light with spatial light modulators* (SPIE Press, 2017) p. 57.

[31] Carmelo Rosales-Guzmán, Xiao-Bo Hu, Adam Selyem,

Pedro Moreno-Acosta, Sonja Franke-Arnold, Ruben Ramos-Garcia, and Andrew Forbes, "Polarisation-insensitive generation of complex vector modes from a digital micromirror device," Sci. Rep. **10**, 10434 (2020).

[32] Eileen Otte and Cornelia Denz, "Customization and analysis of structured singular light fields," J. Opt. **23**, 073501 (2021).

[33] David Foster, Charles Kind, Paul J Ackerman, Jung-Shen B Tai, Mark R Dennis, and Ivan I Smalyukh, "Two-dimensional skyrmion bags in liquid crystals and ferromagnets," Nat. Phys. **15**, 655–659 (2019).

[34] Hiroshi Kuratsuji and Satoshi Tsuchida, "Evolution of the stokes parameters, polarization singularities, and optical skyrmion," Phys. Rev. A **103**, 023514 (2021).

[35] Yijie Shen, "Topological bimeronic beams," Opt. Lett. **4**, 2 (2021).

[36] Mateusz Król, Helgi Sigurdsson, Katarzyna Rechcińska, Przemysław Oliwa, Krzystof Tyszka, Witold Bardyszewski, Andrzej Opala, Michał Matuszewski, Przemysław Morawiak, Rafał Mazur, Wiktor Piecek, Przemysław Kula, Pavlos G. Lagoudakis, Barbara Pietka, and Jacek Szczytko, "Observation of second-order meron polarization textures in optical microcavities," Optica **8**, 255–261 (2021).

[37] Cheng Guo, Meng Xiao, Yu Guo, Luqi Yuan, and Shanhui Fan, "Meron spin textures in momentum space," Phys. Rev. Lett. **124**, 106103 (2020).

[38] Chengkun Song, Yunxu Ma, Chendong Jin, Jinshuai Wang, Haiyan Xia, Jianbo Wang, and Qingfang Liu, "Field-tuned spin excitation spectrum of kπ skyrmion," New J. Phys. **21**, 083006 (2019).

[39] Amber M Beckley, Thomas G Brown, and Miguel A Alonso, "Full poincaré beams," Opt. Express **18**, 10777–10785 (2010).

[40] Xiaohui Ling, Xunong Yi, Zhiping Dai, Youwen Wang, and Liezun Chen, "Characterization and manipulation of full poincaré beams on the hybrid poincaré sphere," JOSA B **33**, 2172–2176 (2016).

[41] Stefano Donati, Lorenzo Dominici, Galbadrakh Dagvadorj, Dario Ballarini, Milena De Giorgi, Alberto Bramati, Giuseppe Gigli, Yuri G Rubo, Marzena Hanna Szymańska, and Daniele Sanvitto, "Twist of generalized skyrmions and spin vortices in a polariton superfluid," PNAS **113**, 14926–14931 (2016).

[42] Dorilian Lopez-Mago, "On the overall polarisation properties of poincaré beams," J. Opt. **21**, 115605 (2019).

[43] Eileen Otte, Christina Alpmann, and Cornelia Denz, "Polarization singularity explosions in tailored light fields," Laser Photonics Rev. **12**, 1700200 (2018).

[44] Ermes Toninelli, Bienvenu Ndagano, Adam Vallés, Bereneice Sephton, Isaac Nape, Antonio Ambrosio, Federico Capasso, Miles J Padgett, and Andrew Forbes, "Concepts in quantum state tomography and classical implementation with intense light: a tutorial," Advances in Optics and Photonics **11**, 67–134 (2019).

[45] Danica Sugic, Ramon Droop, Eileen Otte, Daniel Ehrmanntraut, Franco Nori, Janne Ruostekoski, Cornelia Denz, and Mark R Dennis, "Particle-like topologies in light," Nat. Commun. **12**, 1–10 (2021).